Strong hybridization in vanadium oxides: evidence from photoemission and absorption spectroscopy

1998 J. Phys.: Condens. Matter 10 5697

(http://iopscience.iop.org/0953-8984/10/25/018)

J. Phys.: Condens. Matter **10** (1998) 5697–5716. Printed in the UK PII: S0953-8984(98)89027-9

Strong hybridization in vanadium oxides: evidence from photoemission and absorption spectroscopy

R Zimmermann, R Claessen, F Reinert, P Steiner and S Hüfner
Universität des Saarlandes, FR 10.2—Experimentalphysik, D-66041 Saarbrücken, Germany

Received 5 November 1997, in final form 11 March 1998

Abstract. We present x-ray photoemission spectra of the vanadium oxides V_2O_5, VO_2, and V_2O_3, and their analysis in terms of a simple cluster model based on the Anderson impurity Hamiltonian. The electronic structure of these materials is characterized by a strong V 3d–O 2p hybridization energy which exceeds the energy scales related to on-site Coulomb correlation and metal–ligand charge transfer. This result is at variance with the usual Mott–Hubbard picture, but agrees with recent studies of other early 3d transition metal compounds. The V 3d ground-state occupations obtained by the cluster-model analysis are considerably higher than the values derived from the formal valencies. Covalency also affects the exchange splitting observed in the V 3s core-hole spectra. X-ray absorption measurements and resonant photoemission spectroscopy at the V 2p–3d threshold provide further evidence for a strong V 3d–O 2p coupling.

1. Introduction

3d transition metal oxides (TMOs) show a great variety of electronic and magnetic properties. This is particularly true for the compounds of the early 3d transition metals (TM) from Sc to Cr. As examples we consider here the binary oxides V_2O_3, VO_2, and V_2O_5 of vanadium (atomic electron configuration $3d^34s^2$) with cation valences of 3, 4, and 5, respectively, corresponding to the formal valence shell configurations $3d^2$, $3d^1$, and $3d^0$. V_2O_5 is a diamagnetic insulator with a gap of $\approx$2 eV, as could be expected from the formally empty 3d shell of the V cation [1]. VO_2 undergoes an insulator-to-metal transition with a sudden conductivity increase of almost five orders of magnitude at 340 K [2]. The gap in the insulating low-temperature phase amounts to $\approx$0.5 eV [1]. V_2O_3, crystallizing in the corundum structure, also exhibits an insulator-to-metal transition with a 6–7 orders of magnitude jump in the conductivity at 160 K [3] and a gap of 0.2–0.3 eV in the insulating phase [1].

Despite the many efforts made towards obtaining an understanding of their electronic behaviour, the vanadium oxides still pose many open questions. V_2O_3 for example has often been regarded as prototype for the so-called Mott–Hubbard (MH) compounds [4, 5] with $U_{dd} < \Delta$. Here Δ is the charge-transfer (CT) energy required to transfer an electron from a ligand orbital (e.g. O 2p) to the TM 3d orbital, and U_{dd} is the Coulomb repulsion energy of two 3d electrons. Metallic or insulating behaviour as well as metal–insulator transitions can be analysed in terms of these parameters and their relation to the bandwidths W and w of the O 2p and TM 3d bands, respectively [6, 7]. However, the nature of the phase transition in V_2O_3 and also the influence of the antiferromagnetic ordering on it are still poorly understood [8]. The same applies to VO_2; some authors relate its phase transition to a MH scenario [9], whereas others attribute it to electron–phonon coupling (a Peierls mechanism), on the

0953-8984/98/255697+20$19.50

basis of the change in crystal symmetry from a rutile-type structure above the transition temperature to a strongly distorted rutile structure (of monoclinic symmetry) below it [10].

Whereas the electronic character of the early TMOs is thus still an open question, late TMOs like NiO or CuO [11–13] can be shown to belong to the CT regime of the Zaanen–Sawatzky–Allen (ZSA) phase diagram [4, 14], meaning that it is the CT energy which determines their fundamental excitation gap ($\Delta < U_{dd}$), with covalency being a small (but for some aspects crucial) perturbation.

Estimates of the important model Hamiltonian energies U_{dd} and Δ can be obtained by a cluster-model analysis [15–17] of data from experiments like photoemission, inverse photoemission or x-ray absorption studies. An additional parameter in such an analysis is the hybridization energy (or inverse hopping rate) V of the O 2p and TM 3d orbitals. To be more specific, it is the effective hybridization $V_{eff} = \sqrt{n_h}V$ (n_h being the formal number of holes in the TM 3d shell in a purely ionic picture) which appears in the non-diagonal matrix elements of the Hamiltonian matrix. Previous applications of the cluster model to selected early TMOs [18, 19] have shown that the large number of holes in the 3d shell results in a considerably enhanced value of V_{eff}, which thus becomes comparable to the other parameters or can even dominate the electronic structure, rendering the usual MH description of these compounds highly questionable [20, 21].

In this paper we present core-level spectra of the vanadium oxides V_2O_5, VO_2, and V_2O_3 measured by x-ray photoemission spectroscopy (XPS). The data are modelled by means of simple cluster-model calculations based on the Anderson impurity Hamiltonian (AIH) [22] (neglecting multiplet and crystal-field effects) in order to extract the parameters U_{dd}, Δ, and V_{eff}. The ligand–cation hybridization can also be probed by x-ray absorption spectroscopy (XAS) and resonant photoemission (ResPES) by sweeping the energy of the exciting photon through the threshold energy of a core level. Therefore we have also performed XAS and ResPES measurements at the V 2p and O 1s absorption edges as an independent check of our cluster-model results. All experimental results lead to the unambiguous conclusion that the electronic character of the vanadium oxides studied here is determined by a strong hybridization between V 3d and O 2p orbitals, in agreement with similar results for other early TMOs [19–21, 23, 24]. As a consequence, these compounds cannot be regarded as simple MH systems.

2. Experimental details

2.1. XPS measurements

The room temperature XPS measurements were performed with monochromatized Al Kα radiation ($\hbar\omega = 1486.6$ eV) using an SSI M-Probe Small Spot Spectrometer which is designed to produce photon spots from 1000 μm down to 150 μm. The pass energy setting of the hemispherical analyser and the size of the photon spot were chosen to yield a resolution of $\approx$0.9 eV. The pressure during the angle-integrated measurements was in the low 10^{-10} mbar range.

The position of the Fermi energy E_F was determined using a clean gold sample. The spectra of V_2O_3 and V_2O_5 are directly referred to the instrumental E_F, as the measurements of the former compound were made when it was in the metallic phase, and the latter compound, being semiconducting, showed no charging. Distinct charging was however observed in the insulating phase of VO_2 (at room temperature). Here we aligned the room temperature spectra relative to those measured with the sample in the metallic phase above 340 K in such a way that the Fermi level is placed at the top of the insulator gap ($\approx$0.5 eV).

The resulting energy position corresponds to an effective n-type doping and facilitates better comparison to the other non-metallic oxide, V_2O_5 (see section 3.1.1).

2.2. XAS and ResPES

XAS and ResPES spectra have been measured using synchrotron radiation at the HE-PGM3 monochromator of the BESSY storage ring in Berlin. The photon energy resolution was ≈0.3 eV. The angle-integrated photoemission spectra were taken with the HIRES spectrometer [25] at an overall (electrons and photons) energy resolution of 0.9 eV. The spectra were corrected for features resulting from second-order light. Absolute energy calibration was performed by using the position of the O 2s line and second-order features. An integrated (Shirley) background [26] was subtracted from the raw data. The XAS spectra were measured in the total-yield mode by monitoring the sample current and correcting for variations of the photon flux. The pressure during the room temperature XAS and PE experiments was in the low 10^{-9} mbar range.

2.3. Samples

For all three materials, single crystals were available; only for the XAS measurements on VO_2 was a polycrystalline sample used. *In situ* preparation of clean surfaces started with a slight annealing of the crystals up to ≈150 °C in order to remove water which may sometimes be present in these oxides. Subsequently the VO_2 and V_2O_3 were scraped with a diamond file, whereas the V_2O_5 crystals could be cleaved very easily in the spectrometer due to their layered structure [3]. These procedures resulted in contamination-free surfaces as monitored by the absence of a C 1s signal.

The effect of carbon (oxide) contamination on the PE spectra in the region of the V 2p and O 1s core levels is shown in figure 1 for a V_2O_5 sample. A prominent feature appearing at about 532–533 eV, i.e. on the high-binding-energy side of the O 1s line of the contaminated sample is clearly correlated with the C 1s signal. As the V 2p and O 1s core levels lie so close in binding energy, possible correlation satellites of the V 2p emission can overlap with the O 1s spectrum. Therefore it is crucial to avoid any contamination signal near the O 1s line that could obscure or be mistaken for an intrinsic V 2p satellite.

3. Results and discussion

3.1. X-ray photoemission

3.1.1. Valence band spectra. Figure 2 shows the Al Kα valence band photoemission (PE) spectra for the three vanadium oxides studied. The data have been corrected for an integrated (Shirley) background [26]. The valence bands are separated into a main part covering the binding energy range from 3 to 9 eV and a separate small peak near the Fermi level, which is absent for V_2O_5 and then grows in intensity with the formal d^1 and d^2 occupation in the other two oxides. Therefore it would be tempting to interpret the valence band spectra in terms of a simple ionic picture, namely to assign the main part to the filled O 2p shell and the structure at low binding energy to the increasing number of V 3d electrons. However, as we will show in the course of this paper, there is considerable hybridization which mixes the orbital character of these spectral features.

The binding energy of the onset of the valence band in V_2O_5 coincides with the optical gap energy of 2 eV [1], implying that the Fermi energy is pinned near the bottom of

the conduction band, presumably due to a small concentration of oxygen defects leading to electron doping. V_2O_3 is a metal at room temperature and thus clearly exhibits finite spectral weight at the Fermi energy. As mentioned before, VO_2 displayed strong charging below 340 K, so the spectrum was aligned in such a way as to place the Fermi level at the top of the small energy gap. Apart from as regards the charging, no differences between the insulating and metallic phase could be resolved within the instrumental resolution.

3.1.2. Core-level spectra. Figure 3 displays the V 2s, V 2p, and V 3p core-level spectra of the three oxides, in comparison. Figure 4 shows in addition the V 3s spectra. All of the data were taken at room temperature, so VO_2 was in the insulating phase and V_2O_3 in the metallic phase. For VO_2 we also took some spectra for the metallic phase (not shown here) at $\approx$100 °C, but due to the limited instrumental resolution no differences from the spectra for the insulating phase (except as regards charging) could be detected.

The widths of the core spectra are found to increase from the (formally) d^0 system V_2O_5 to the d^1 system VO_2 and finally to V_2O_3 with formally two electrons in the V 3d shell. This behaviour can be explained by there being a growing number of available (and here unresolved) multiplet configurations in the corresponding PE final states, resulting from the coupling of the core hole to the 3d valence electrons. With a formally empty 3d shell, V_2O_5 will thus display no multiplet splitting which explains the sharpness of its core-level peaks. The effect of the multiplet splitting, in VO_2 and V_2O_3 is particularly strong in the V 3p spectra (panel (c) of figure 3) due to the large spatial overlap with the 3d shell, also giving contributions to the features centred at around 52–54 eV. The small spin–orbit splitting of

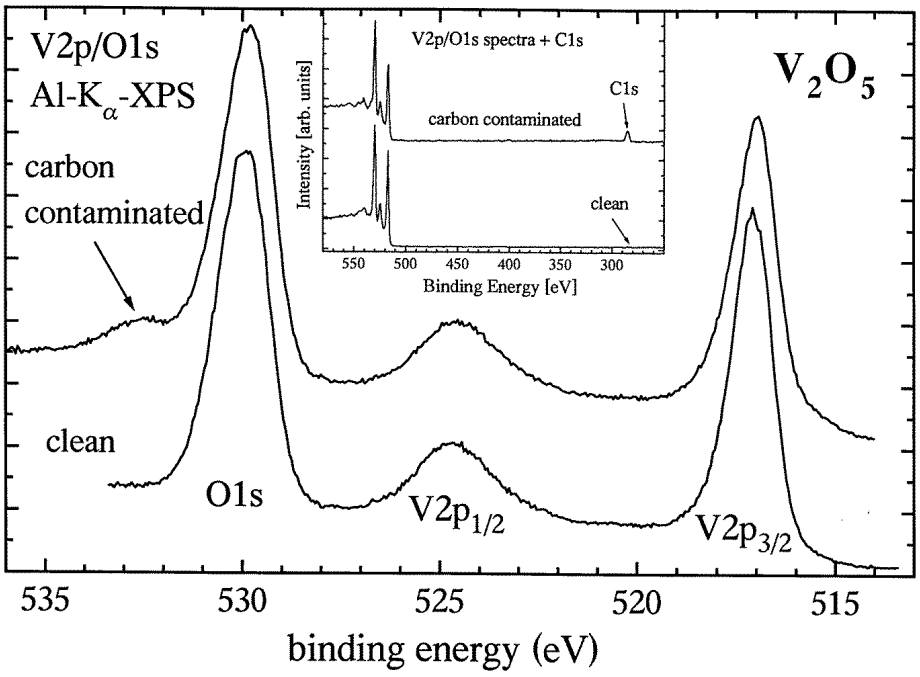

Figure 1. The influence of the carbon (oxide) contamination on the V 2p/O 1s spectra of vanadium oxides, here shown for the case of V_2O_5 as an example. The inset shows the corresponding V 2p/O 1s spectra including the binding energy range of the C 1s core level.

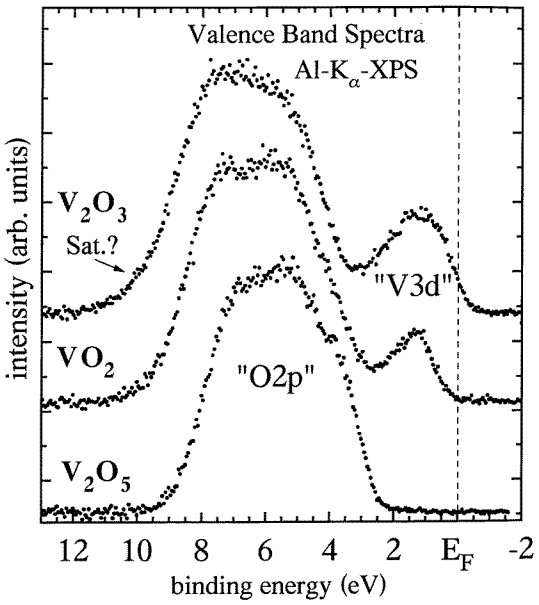

Figure 2. Shirley background-corrected valence band XPS spectra of V_2O_3, VO_2, and V_2O_5, taken at room temperature and normalized to equal heights.

the V 3p spectrum of only 1 eV is not resolved, and contributes to the overall broadening.

The large width of the V 2s lines (panel (a) in figure 3) as compared to the core levels at lower binding energies is attributed to a substantially larger lifetime broadening. The V 2p spectrum (panel (b)) is spin–orbit split into the $2p_{3/2}$ and $2p_{1/2}$ parts, separated by 7–8 eV, and this doublet is followed by the O 1s emission at $E_B \approx 530$ eV. Apparently, the asymmetry on the high-binding-energy side of the O 1s line increases in going from V_2O_5 to V_2O_3. Due to this systematic trend and the complete absence of a C 1s signal, which would otherwise relate the asymmetry to a possible surface contamination (cf. figure 1), we interpret it as part of the intrinsic satellite structure of the V 2p spectrum (see section 3.1.3).

The interaction of the core hole with the 3d valence shell not only causes a broadening of the lines but also results in satellite structures which can be found in most of the spectra in figures 3 and 4. The separation from the corresponding main lines is typically 14–15 eV for V_2O_5 and 10–13 eV for VO_2 and V_2O_3. From the main-line–satellite separation in the V 2s, V 3s, and V 3p spectra we can estimate the satellite positions in the V 2p spectra, where they interfere with the spin–orbit splitting and the O 1s emission. One finds that for V_2O_5 a satellite belonging to the V $2p_{3/2}$ main line and for VO_2 and V_2O_3 a satellite of the V $2p_{1/2}$ line could be expected on the high-binding-energy side of the O 1s peak leading to the asymmetry seen at ≈531 eV. For the latter two oxides, the satellite of the V $2p_{3/2}$ part falls into the binding energy range of the V $2p_{1/2}$ line. The V $2p_{1/2}$ satellite in V_2O_5 contributes to a structure at around 540 eV (not shown here), which however could also be interpreted as a plasmon satellite of the O 1s peak [27].

The main-line–satellite separations ΔE_{sat} and relative satellite intensities I_{sat}/I_{main} have been extracted from least-squares fits to the experimental data (using a combination of Gaussian and Lorentzian line profiles [28]) and are listed in table 1. The estimated uncertainties for ΔE_{sat} are approximately 0.5 eV for the analysis of the V 2s, 3s, and 3p spectra, and 1.0 eV for the V 2p spectra. For I_{sat}/I_{main} we estimate an accuracy of about

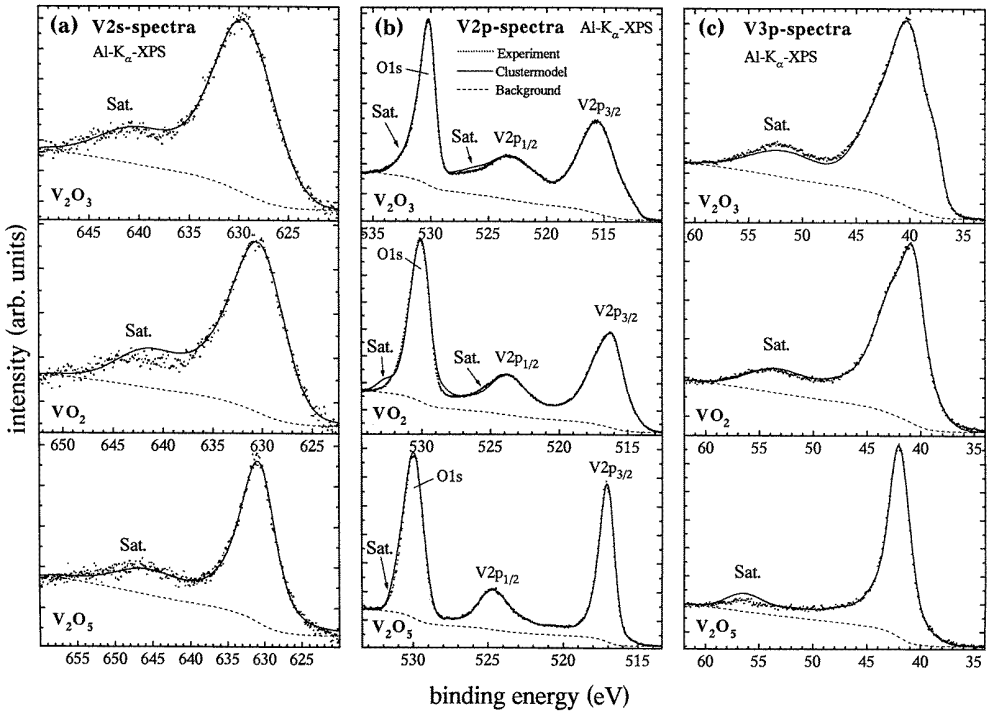

Figure 3. Core-level XPS spectra of the vanadium oxides V_2O_3, VO_2, and V_2O_5. (a), (b), and (c) show the V 2s, V 2p, and V 3p spectra, respectively. Solid lines correspond to the results of the cluster-model calculation (see the text), and dashed lines indicate a Shirley-type inelastic background. 'Sat.' marks the correlation satellite features.

Table 1. Main-line–satellite separations ΔE_{sat} and satellite intensities relative to the main-line intensities I_{sat}/I_{main} for the V 2s, V 2p, V 3s, and V 3p core-level spectra (figures 3 and 4) of V_2O_5, VO_2, and V_2O_3.

	V_2O_5		VO_2		V_2O_3	
	ΔE_{sat} (eV)	I_{sat}/I_{main}	ΔE_{sat} (eV)	I_{sat}/I_{main}	ΔE_{sat} (eV)	I_{sat}/I_{main}
V 2s	15.0	0.20	11.6	0.12	10.7	0.19
V $2p_{1/2}$	—	—	8.3	0.12	9.7	0.19
V $2p_{3/2}$	14.1	0.06	10.2	0.11	11.4	0.17
V 3s	—	—	13.0	0.03	13.0	0.06
V 3p	13.9	0.07	11.3	0.16	10.5	0.25

0.01 for V 3s, 0.03 for V 2s and 3p, and 0.05 for V 2p.

From table 1 it can be seen that the interpretation of the O 1s asymmetry as an intrinsic satellite structure is not unambiguous, since for VO_2 and V_2O_3 it results in a separation of the V $2p_{1/2}$ satellite from the corresponding main line which is distinctly smaller than that for the V $2p_{3/2}$ satellite. On the other hand, the relative satellite-to-main-line intensity ratios of the two spin–orbit parts are found to be rather similar. However, it should be noted here that, due to the broad and overlapping features in the V 2p spectra, the corresponding fit parameters carry a non-negligible error bar. Table 1 also shows that the 3s satellite is less

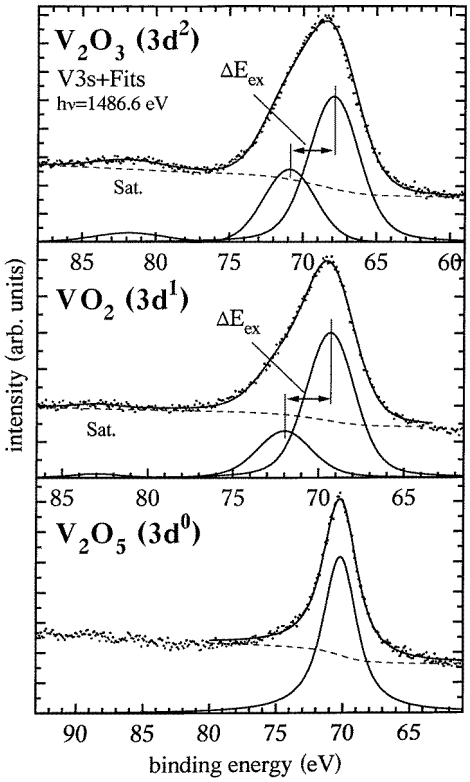

Figure 4. V 3s PE spectra of the vanadium oxides V_2O_3, VO_2, and V_2O_5. Least-squares fits to the experimental data (see the text) are shown as solid lines, and the Shirley background is indicated by dashed lines. 'Sat.' again marks the correlation satellite.

intense than those for the other core levels; for V_2O_5 it is hardly observable at all.

Satellite structures were not observed in the XPS valence band spectra (see figure 2) and are therefore not further discussed in the following. We only note that the less steep slope on the high-energy side of the O 2p band for V_2O_3 as compared to V_2O_5 may originate from a small satellite at around 10.5 eV.

3.1.3. Cluster-model description. In this section the vanadium core-level spectra are analysed on the basis of a simple cluster model [13, 15–17], in which multiplet and crystal-field effects are neglected. The electronic structure of a system consisting of a 3d transition metal cation and its surrounding ligand anions can be described by the interactions between and within the corresponding valence shells, i.e. in our case in terms of the V 3d orbitals (d) and O 2p-derived ligand states (L) symmetrized according to the local cluster configuration. The Hamiltonian, which is a simplified version of the AIH, then assumes the form

$$H_{cm} = \epsilon_L \sum_{\nu=1}^{N_d} L_\nu^+ L_\nu + \epsilon_d \sum_{\nu=1}^{N_d} d_\nu^+ d_\nu + \epsilon_c c^+ c + \frac{1}{2} U_{dd} \sum_{\substack{\nu,\mu=1 \\ \nu\neq\mu}}^{N_d} d_\nu^+ d_\nu d_\mu^+ d_\mu + V \sum_{\nu=1}^{N_d} (d_\nu^+ L_\nu + L_\nu^+ d_\nu) - U_{cd}(1 - c^+ c) \sum_{\nu=1}^{N_d} d_\nu^+ d_\nu \qquad (1)$$

where the L_ν^+, L_ν and d_ν^+, d_ν are creation and annihilation operators for an electron in a ligand orbital and a V 3d orbital, respectively. c^+ and c create and annihilate the core electron. The indices ν and μ represent coupled labels for orbital and spin symmetry, and N_d denotes the degeneracy of the V 3d orbital. As our simple model neglects crystal-field and multiplet effects, we have to take $N_d = 10$. The first three terms in (1) describe the one-electron energies of the ligand (O 2p), 3d transition metal, and core orbitals, respectively. The fourth term contains the effect of the Coulomb repulsion U_{dd} on the metal atom. The hybridization V mixes V 3d and symmetrized ligand orbitals. The last term accounts for the effect of the core-hole potential generated by photoemission of a vanadium core electron.

Diagonalizing H_{cm} in the basis sets $\{|\mathrm{d}^{n+q}\underline{\mathrm{L}}^q\rangle\}$ and $\{|\underline{\mathrm{c}}\mathrm{d}^{n+q}\underline{\mathrm{L}}^q\rangle\}$ for the initial and photoemission final states, respectively, yields the corresponding eigenvalues and eigenstates, with the latter being of the form

$$|\psi_g\rangle = \sum_{q=0}^{10-n} \alpha_{gq}|\mathrm{d}^{n+q}\underline{\mathrm{L}}^q\rangle \tag{2}$$

for the ground state (the lowest-energy initial state) and

$$|\psi_j\rangle = \sum_{q=0}^{10-n} \beta_{jq}|\underline{\mathrm{c}}\mathrm{d}^{n+q}\underline{\mathrm{L}}^q\rangle \qquad j \in \{0, \ldots, 10-n\} \tag{3}$$

for the final states. Here n is the formal occupation of the V 3d shell in a purely ionic picture (e.g. $n = 2$ for V_2O_3), $\underline{\mathrm{L}}$ means a hole in the ligand valence orbital (O 2p), and $\underline{\mathrm{c}}$ stands for a core hole in the final state of the photoemission process. On the basis of the sudden approximation for the photoelectron current [29], theoretical satellite intensities, main-line–satellite separations, and occupation numbers (using the occupation probabilities $|\alpha_{gq}|^2$ and $|\beta_{jq}|^2$) can be calculated using the model parameters Δ, U_{dd}, U_{cd}, and V as input. A nice description of how different kinds of excitation spectra (photoemission, inverse PE, energy-loss spectra) can be calculated within the cluster limit of the AIH has been given by Imer and Wuilloud in reference [30], to which the interested reader is referred for details.

In our calculations, all of the basis states $|\mathrm{d}^{n+q}\underline{\mathrm{L}}^q\rangle$ for the initial state and $|\underline{\mathrm{c}}\mathrm{d}^{n+q}\underline{\mathrm{L}}^q\rangle$ for the final state have been included (i.e. $q = 0, \ldots, 10-n$). We tried to reproduce all of the core-level spectra of a given oxide with the same set of parameters Δ, U_{dd}, and V_i (hybridization in the initial state); only V_f (hybridization in the final state) and U_{cd} were allowed to vary slightly between different core levels, the latter by using the relation $U_{cd} = U_{dd}/\gamma$ with $\gamma \approx 0.8$ for 2s and 2p core holes and $\gamma \approx 0.9$ for 3p PE [23], as deduced from atomic values based on the Slater–Condon parameters [31]. Note that U_{cd} is a positive parameter, as defined in (1). We found that with such a 'universal' choice of parameters the calculated satellite separations and intensities did not in all cases reproduce the experimental data in an optimal way. This may well result from the neglect of multiplet and crystal-field interactions in our simple approach. Though we can thus not expect to model all details of the spectra, it should still be possible to reproduce the essential features and trends in the electronic structure of the vanadium oxides.

Figure 3 compares the results of the cluster-model calculations for the core-level spectra with the experimental data. The theoretical spectra were produced from the calculated satellite separations and intensities, with the line broadening taken from the above-mentioned Gaussian–Lorentzian fits of the measured data. We omit a similar presentation for the V 3s spectra, since the cluster model was not able to reproduce—with reasonable parameters—the very low satellite intensities seen in the experimental spectra (cf. figure 4 and table 1). This problem could be related to configuration interaction between the 3s PE final states

$3s^1 3p^6 3d^n$ and $3s^2 3p^4 3d^{n+1}$ which is not contained in our model but has been shown to additionally affect the 3s satellite structure in early 3d TMOs [32, 33].

Table 2. Cluster-model parameters Δ, U_{dd}, and V_i for the vanadium oxides V_2O_5, VO_2, and V_2O_3. The last two columns contain the effective initial-state hybridization $V_i^{eff} = \sqrt{n_h} V_i$ and the formal number n_h of 3d holes, respectively.

	Δ (eV)	U_{dd} (eV)	V_i (eV)	V_i^{eff} (eV)	n_h
V_2O_5	3.5	4.5	3.6	11.4	10
VO_2	4.4	3.8	2.5	7.5	9
V_2O_3	5.5	3.8	2.3	6.5	8

The parameter values, satellite separations and intensities (in comparison with experiment), and the 3d occupation numbers of the ground state (n_g), main line (n_m), and satellite line (n_{sat}) obtained from the cluster-model analysis are presented in tables 2 and 3. Figure 3 and table 3 demonstrate that the model is—despite its simplicity—quite able to satisfactorily reproduce the measured PE excitation spectra.

Our analysis yields for the charge transfer and d–d excitation energies Δ and U_{dd} typical values of 4–5 eV, whereas the effective initial-state hybridization V_i^{eff} is found to be significantly larger, ranging from nearly 7 to 12 eV. Due to the effect of the core-hole potential, the hybridization is additionally increased ($V_f^{eff}/V_i^{eff} \approx 1.0$–$1.3$) in the PE final state. These results indicate that the electronic structure of the vanadium oxides is dominated by a strong coupling between the V 3d and the O 2p ligand orbitals, a situation which strongly differs from that found in late TMOs [11–13, 34, 35]. The error bars for the hybridization parameters are only a few tenths of an eV. The uncertainties for Δ and U_{dd} are somewhat larger; however, they do not profoundly affect the gross electronic structure as long as the hybridization dominates the other terms. The parameter values obtained from our analysis are comparable to those presented in previous cluster-model studies available for V_2O_5 [23], VO_2 [19], and V_2O_3 [23, 24].

Table 3. Cluster-model parameters U_{cd}, V_f, and the effective final-state hybridization $V_f^{eff} = \sqrt{n_h} V_f$ for V 2s, V 2p, and V 3p core-level photoemission. Also listed are the satellite separations and relative intensities obtained from the cluster model (ΔE_{sat}^{CM}, I_{sat}^{CM}/I_{main}) in comparison with the experimental values (ΔE_{sat}^{exp}, I_{sat}^{exp}/I_{main}), and occupation numbers of the ground state (n_g) and photoemission final states (main line, n_m, and satellite, n_{sat}) compared with the formal value n_d for V_2O_5, VO_2, and V_2O_3. All of the energies are given in eV.

		V_f	V_f^{eff}	U_{cd}	n_d	n_g	n_m	n_{sat}	ΔE_{sat}^{CM}	ΔE_{sat}^{exp}	I_{sat}^{CM}/I_{main}	I_{sat}^{exp}/I_{main}
V_2O_5	2s	3.9	12.3	5.9	0	1.3	2.1	2.1	14.7	15.0	0.19	0.20
	2p	3.6	11.4	5.3			2.0	2.0	13.9	14.1	0.13	0.06
	3p	3.6	11.4	5.0			1.9	1.9	13.9	13.9	0.12	0.07
VO_2	2s	2.6	7.8	4.5	1	1.9	2.5	2.6	10.1	11.6	0.16	0.12
	2p	2.5	7.5	4.4			2.5	2.5	9.8	9.3*	0.14	0.11*
	3p	2.9	8.7	4.2			2.6	2.6	11.0	11.3	0.18	0.16
V_2O_3	2s	2.8	7.9	4.5	2	2.6	3.3	3.4	10.3	10.7	0.21	0.19
	2p	2.8	7.9	4.5			3.3	3.4	10.3	10.5*	0.21	0.18*
	3p	2.9	8.2	4.3			3.3	3.4	10.6	10.5	0.21	0.25

* Mean values from $2p_{3/2}$ and $2p_{1/2}$ satellites (see table 1).

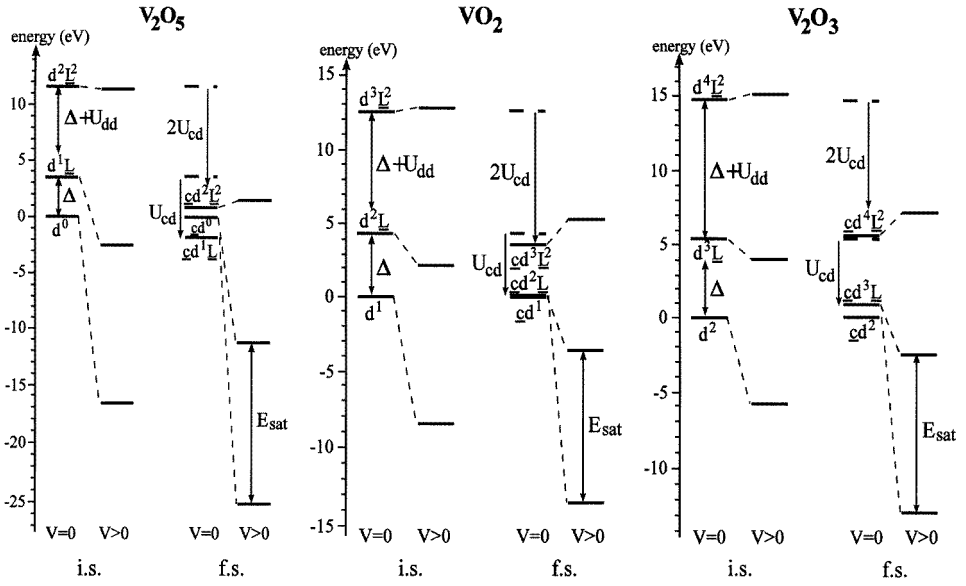

Figure 5. Energy level diagrams for the vanadium oxides V_2O_5, VO_2, and V_2O_3 calculated by the cluster model described in the text. Shown are basis states and eigenstates of the initial-state (left-hand panel) and V 2p PE final-state Hamiltonian (right-hand panel). The dramatic effects of the hybridization V are clearly visible.

Figure 5 shows the energy levels of the (unhybridized) basis states compared to those of the initial and V 2p PE final states as calculated using the cluster model. The marked deviation of the eigenstates from the basis states directly reflects the effect of the hybridization. It is largest for V_2O_5 not only due to the large number of holes in the V 3d shell, but also because the bare hybridization parameter V_i (and also V_f) is already bigger than in the other oxides, in accordance with the smaller mean V–O bond length in the pentoxide [3].

The strong mixing between the V 3d and O 2p levels is also reflected in an enhancement of the ground-state and final-state V 3d occupation numbers (n_g, n_m, and n_{sat}) relative to their values in a purely ionic picture. For n_g we obtain 1.3, 1.9, and 2.6 instead of the formal occupations 0, 1, and 2 for V_2O_5, VO_2, and V_2O_3, respectively. In the final states (both main line *and* satellite) the deviation is even larger, with e.g. V 2p main-line occupations of 2.0, 2.5, and 3.3, respectively. This increase of the 3d occupation in the final state is partly induced by the core-hole potential U_{cd} which lowers the energy of the V 3d states. For a given compound the final-state occupation numbers do not vary much between the main line and satellite or between the different core excitations.

A more detailed analysis of the cluster-model results shows that the large 3d occupation numbers originate from the fact that the configurations $|\mathrm{d}^{n+q}\underline{\mathrm{L}}^q\rangle$ (initial state) or $|\underline{\mathrm{c}}\mathrm{d}^{n+q}\underline{\mathrm{L}}^q\rangle$ (final state) with q up to 4 contribute considerably to the resulting eigenstates. This is illustrated in figure 6, where the occupation probabilities $|\alpha_{gq}|^2$ and $|\beta_{jq}|^2$ (cf. equations (2) and (3)) of the different basis states in the ground state $|\psi_g\rangle$ and in the final states $|\psi_m\rangle$ (main line) and $|\psi_{sat}\rangle$ (satellite) are sketched for the example of V 2p photoemission. For the other core-level excitations, one finds similar distributions. Figure 6 clearly demonstrates that the PE final states of the vanadium oxides can no longer be characterized by a single dominant ionic configuration $|\underline{\mathrm{c}}\mathrm{d}^{n+q}\underline{\mathrm{L}}^q\rangle$, as is possible for the late TM compounds.

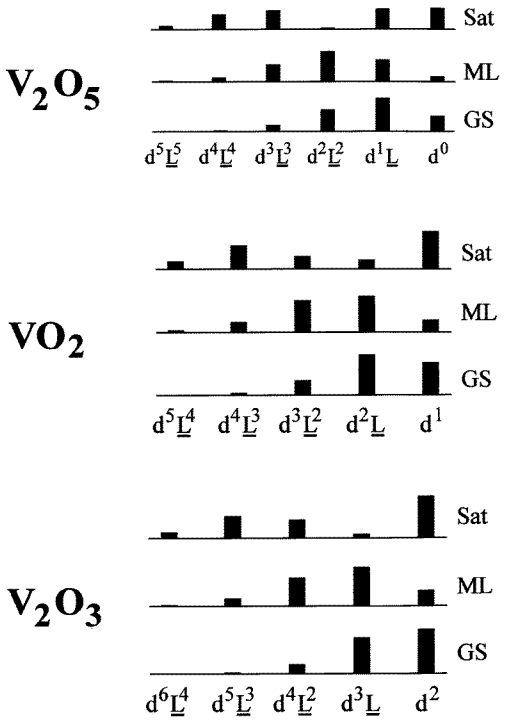

Figure 6. The fractional parentage of the various basis states in the ground state (GS) $|\psi_g\rangle$ and the PE final states $|\psi_m\rangle$ (ML = main line) and $|\psi_{sat}\rangle$ (Sat = satellite), obtained from the cluster model for the case of V 2p PE.

Another method for obtaining at least a rough estimate of the 3d occupation numbers is the analysis of Auger spectra involving the 3d shell, e.g. the 2p3p3d and 2p3d3d decays. Such transitions should only be observable if the 3d shell is not empty, because the Auger excitation is regarded as a local process, with interatomic transitions being negligible to a first approximation [36]. As regards the 2p3d3d Auger decay, the evaluation of its intensity in the formal d^0 compound $KMnO_4$, for example, yielded an apparent 3d occupation of the Mn^{7+} cation of about five electrons [37]. Although the exact number has to be viewed with caution due to the effects of the core-hole potential in the intermediate state, the result nevertheless indicates a strongly non-zero 3d occupation. The same was found for the d^0 systems TiO_2 and $PbCrO_4$ [27]. Thus, it comes as no surprise that V_2O_5 also displays an intense 2p3d3d Auger signal (see also section 3.2.2), in good agreement with the finite 3d occupation derived in the cluster-model analysis.

A more quantitative analysis of the Auger spectra of vanadium oxides has been performed by Sawatzky and Post [38] who extracted from a comparison of the 2p3p3d intensities 3d occupation numbers of 2.5, 2.6, and 3.1 for V_2O_5, VO_2, and V_2O_3, respectively. These values are in rather good agreement with the above-stated numbers (2.0, 2.5, and 3.3) for the final state of the V 2p PE, indicating that it is actually the 3d occupation of the *intermediate* (i.e. core-hole-excited) state rather than that of the ground state which is determined by Auger spectroscopy. The authors attributed one of the features of the Auger spectra to V 3d states mixed into the 'O 2p' part of the valence band. Its occurrence and relatively high intensity yield further evidence for a strong hybridization between O 2p and

V 3d states.

3.1.4. Exchange splitting of V 3s photoemission spectra. We finally focus on the V 3s spectra (cf. figure 4), for which a detailed cluster-model analysis was not performed due to the surprisingly low satellite intensity, as discussed above. Nonetheless, these spectra contain other interesting final-state effects, which are related to exchange coupling of the 3s electrons and the valence shell.

In a 3d TM compound, the coupling of the spin of the 3s photohole with the total spin S of the partially filled 3d shell is expected to cause an exchange splitting of the 3s PE line corresponding to high-spin ($S + \frac{1}{2}$) and low-spin ($S - \frac{1}{2}$) final-state configurations [39, 40]. In an ionic picture with integral d occupation, the magnitude of the separation is, according to van Vleck [41], given by

$$\Delta E_{ex} = \begin{cases} J(2S+1) & S \neq 0 \\ 0 & S = 0 \end{cases} \tag{4}$$

where S denotes the total spin of the 3d shell. J is an exchange-coupling constant which is related to the Slater–Condon parameter $G^2(3s, 3d)$ through [42]

$$J = \frac{G^2(3s, 3d)}{5}. \tag{5}$$

Due to correlation and screening effects in the solid, the effective magnitude of $G^2(3s, 3d)$ is often reduced by a factor of ≈ 0.5 relative to its bare atomic value [39]. The intensity ratio of the two exchange-split final-state structures is given by

$$\frac{I(S-\frac{1}{2})}{I(S+\frac{1}{2})} = \frac{S}{S+1}. \tag{6}$$

This theory has been quite successful as regards the interpretation of the 3s spectra of late TM compounds [39, 40] where ΔE_{ex} was found to scale with the 3d occupation (or rather 3d hole number), which in these materials directly correlates with the 3d spin of the ground state. For the vanadium oxides we find however notable deviations from this picture.

Table 4. The exchange splitting ΔE_{ex} and intensity ratio $I(S-1/2)/I(S+1/2)$ as deduced from the fits in figure 4 for the vanadium oxides V_2O_5, VO_2, and V_2O_3. $S/(S+1)$ is the theoretical intensity ratio according to (6). n_d is the formal 3d occupation, and S the total 'Hund's rule spin' of the 3d shell.

	n_d	S	ΔE_{ex} (eV)	$I(S-1/2)/I(S+1/2)$	$S/(S+1)$
V_2O_5	0	0	0	—	0
VO_2	1	$\frac{1}{2}$	2.7	0.36	0.33
V_2O_3	2	1	3.0	0.47	0.5

We begin our discussion with the 3s spectrum of the d^0 compound V_2O_5 which, in contrast to V_2O_3 and VO_2, shows a clear single-line character, i.e. $\Delta E_{ex} = 0$ (see figure 4). According to equation (4), this is indeed the behaviour expected for the formal Hund's rule spin $S = 0$. On the other hand, it should be recalled that the cluster-model analysis for this compound yielded a 3d ground-state occupation number of 1.3. This indicates that one must not take the exchange splitting as a measure of the 3d occupancy, in marked contrast to the case for the late TM oxides. The absence of a measurable 3s exchange splitting has

also been observed for other d^0 systems (e.g. TiO_2 or $KMnO_4$ [27, 37]), despite an actual non-zero d occupation of their respective ground states. This confirms experimentally that in diamagnetic systems the total spin $S = 0$ of the 3d valence shell as derived from the formal valence is conserved under the influence of covalency between 3d and ligand orbitals, since hybridization cannot mix magnetic states into an unmagnetic ionic ground state.

A non-zero exchange splitting is observed in the 3s spectra of VO_2 and V_2O_3, which can be well fitted by a double-peak structure (CT satellites not being included), with the respective intensity ratios in good agreement with equation (6) (see figure 4 and table 4). For V_2O_3 this behaviour is in qualitative agreement with the existence of a local moment ($m = 2.37$ Bohr magnetons) in the metallic phase, inferred from the Curie behaviour of the magnetic susceptibility [43]. The 3s exchange splitting in V_2O_3 has in fact recently been used to monitor the variation of the local moment through the metal–insulator transition [44].

For VO_2 however the situation is more complicated. The 3s spectrum clearly indicates an exchange splitting not much smaller than that observed for V_2O_3. On the other hand, the susceptibility of VO_2 is (in both phases) almost temperature independent [45], and cannot be interpreted in terms of a local moment. This apparent discrepancy can be related to the fact that 3s photoemission and susceptibility measurements probe different spatial scales (and timescales). For example, the 3s core hole excited by photoemission experiences an instantaneous, truly local, on-site 3d spin, whereas the 'local' moment inferred from the Curie behaviour of the susceptibility is a property of the entire cluster consisting of the TM ion and its ligand shell, especially if covalency couples them strongly. Solid-state effects may even completely screen out any local moment behaviour in the global magnetization, despite the observation of a 3s exchange splitting, as found here and in other 3d compounds [46].

Therefore, the 3s exchange splitting observed in these oxides neither directly reflects the 3d occupancy nor necessarily reflects the magnetic behaviour seen in the susceptibility, in contrast to the case for late 3d TM compounds, for which ionic configurations are stabilized due to the reduced role of the covalency. A similar lack of correlation between 3s photoemission exchange splittings and magnetic measurements has been reported in an extensive study of Fe compounds [46]. On the other hand, the systematic variation of ΔE_{ex} observed through the phase transition of V_2O_3 [44] indicates that there is some magnetic information contained in the 3s spectra, whose detailed interpretation however requires further theoretical clarification.

3.2. XAS and ResPES

For a further verification of our cluster-model results on a strong V 3d–O 2p coupling, we also performed XAS and ResPES measurements. For a given configuration d^n of the valence shell, the ResPES effect can be described as an interference of the direct PE process

$$\mathrm{cd}^n + \hbar\omega \rightarrow \mathrm{cd}^{n-1} + \mathrm{e}^- \tag{7}$$

with a second excitation channel

$$\mathrm{cd}^n + \hbar\omega \rightarrow \left[\underline{\mathrm{c}}\mathrm{d}^{n+1}\right]^* \rightarrow \mathrm{cd}^{n-1} + \mathrm{e}^- \tag{8}$$

which leads to the same final state when the photon energy $\hbar\omega$ is swept through the absorption threshold of a core level c. The first step in (8) describes the absorption of the photon resulting in an excited intermediate state, indicated by the asterisk, which decays in the second step through a Coster–Kronig (CK) or super-Coster–Kronig (SCK) process.

Coherent superposition of channels (7) and (8) can lead to a resonant enhancement of the d^{n-1} final state, especially if the cross-section for the absorption process is strong ('giant resonance'). Due to the local character of the ResPES process, it is possible to distinguish TM 3d-like states in the valence band from those having ligand character. If the d^n configuration makes the major contribution to the ground-state wavefunction, ResPES further allows one to separate d^{n-1}-like final states from those with larger $d^n\underline{L}$ contribution [47]. But the strong mixing between the different configurations $d^{n+q}\underline{L}^q$ already existing in the ground state for the vanadium oxides (see figure 6) makes such an analysis rather meaningless for these compounds.

Previous ResPES experiments on vanadium oxides performed at the V 3p threshold [48, 49] already suggested a strong V 3d admixture with the O 2p part of the valence band spectra. Due to the much larger cross-section for TM 2p photoabsorption as compared to the TM 3p edge, one can expect a higher resonant enhancement in ResPES measurements near the 2p threshold. In the following we present such data for V_2O_5 and V_2O_3.

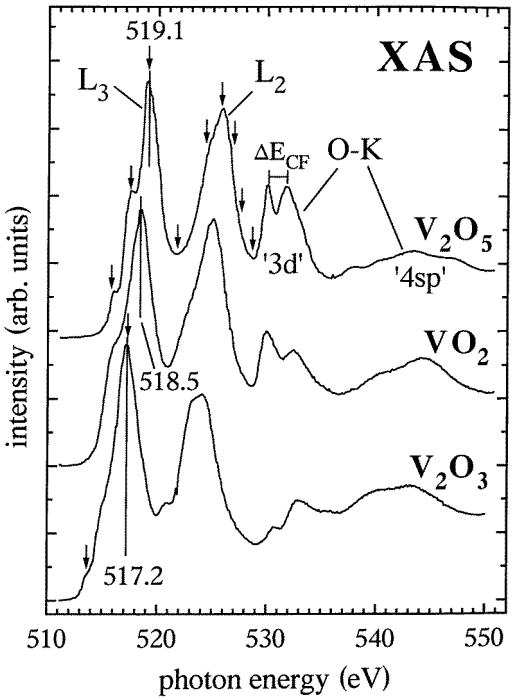

Figure 7. V L_{23}/O K absorption spectra of the vanadium oxides V_2O_5, VO_2, and V_2O_3. ΔE_{CF} denotes the crystal-field splitting of the O 2p ligand states hybridized with V 3d states. The arrows indicate the photon energies used for the ResPES experiments illustrated in figure 9, later.

3.2.1. V L_{23}/O K XAS. Figure 7 shows the V L_{23}/O K absorption spectra for the three vanadium oxides V_2O_5, VO_2, and V_2O_3, taken with an angle of 60° between the surface normal and the direction of light incidence. The overall shape of the spin–orbit-split V L_{23} absorption is determined by the intra-atomic interaction of the absorption final state (multiplets) as well as by crystal-field (CF) effects [50].

Since the absorption process is a local (i.e. intra-atomic) excitation whose probability is, in principle, proportional to the unoccupied partial density of states, we should in a purely ionic picture with fully occupied O 2p orbitals not expect to see any O K absorption at all. The experiment, in contrast, shows a quite noticeable O K absorption signal in the higher-energy region of figure 7, indicating the existence of a large number of unoccupied O 2p states due to pronounced hybridization-induced transfer of O 2p electrons into V 3d and V 4sp orbitals.

The first part of the O K absorption spectrum, centred at around 532 eV, is attributed to O 2p states hybridized with unoccupied V 3d states, and the structure centred at around $\hbar\omega \approx 543$ eV arises from O 2p states hybridized with V 4sp states [51]. The double-peaked feature of the former has its origin in the (distorted) octahedral crystal field, which splits the 3d states in a lower-lying t_{2g} and a higher-lying e_g part [51]. For the case of V_2O_5 one may argue about whether the coordination of the V ion can still be described by a strongly distorted octahedron, but crystal-field effects are clearly present. For a detailed interpretation of the observed features, we refer the reader to the literature [20, 50–55].

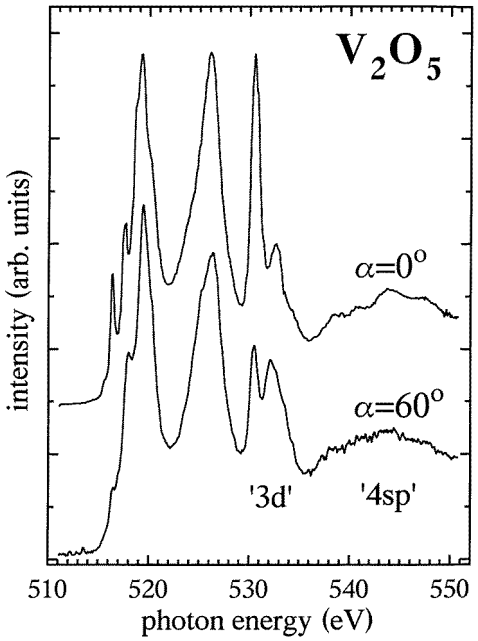

Figure 8. V L_{23}/O K absorption spectra of V_2O_5 taken for different angles α between the surface normal and the direction of light incidence.

Figure 8 shows, using V_2O_5 as an example, that the intensity ratio of the CF-split parts also depends on the angle α between the direction of light incidence and the surface normal. This effect is caused by the variation of the polarization vector of the light relative to the different orientations of the 3d orbitals in the layered crystal structure of V_2O_5 [52]. However, for our further analysis it is important to note that we find the *mean* intensity of the V 3d part of the O K edge, i.e. averaged over the crystal-field terms and normalized to the corresponding V L_{23} intensity, to be fairly independent of the light incidence angle α. For V_2O_5, the corresponding absorption ratios are 0.22 and 0.24 for $\alpha = 60^\circ$ and 0°, respectively. For the other oxides with their much more isotropic crystal structure,

the absorption spectra showed only a marginal polarization dependence [27]. With this empirical result that geometry effects are apparently negligible, we take the total 'V 3d-like' O K absorption weight in our XAS spectra as a measure for the number $n^{\mathrm{h}}_{\mathrm{O\,2p}}$ of those holes in the O 2p ligand shell which are caused by hybridization with the V 3d states.

On the basis of these considerations, one can now perform a quantitative comparison of the absorption data to the results of the cluster-model analysis of the PE core-level spectra. For this purpose, we assume that for an oxide of composition $\mathrm{V}_a\mathrm{O}_b$ the (V 3d-like) O K absorption signal is given by

$$I(\mathrm{O_K}) \propto \sigma_{\mathrm{O\,1s}} b n^{\mathrm{h}}_{\mathrm{O\,2p}} \tag{9}$$

with $\sigma_{\mathrm{O\,1s}}$ denoting the O 1s photoabsorption cross-section and $n^{\mathrm{h}}_{\mathrm{O\,2p}}$ as defined above. Similarly, one has for the V L_{23} absorption

$$I(\mathrm{V_{L_{23}}}) \propto \sigma_{\mathrm{V\,2p}} a(10 - n_g) \tag{10}$$

where $\sigma_{\mathrm{V\,2p}}$ is the photoabsorption cross-section for the V 2p core level and $(10 - n_g)$ is the number of holes in the V 3d shell with ground-state occupation number n_g. The number of '3d-like' O 2p holes $n^{\mathrm{h}}_{\mathrm{O\,2p}}$ can easily be determined from the requirement of charge neutrality in the compound, leading to

$$a(n_g - n_d) = b n^{\mathrm{h}}_{\mathrm{O\,2p}} \tag{11}$$

where n_d is the 3d occupation expected from the formal vanadium valence. The intensity ratio $I(\mathrm{O_K})/I(\mathrm{V_{L_{23}}})$ calculated from equations (9) and (10) using $n^{\mathrm{h}}_{\mathrm{O\,2p}}$ from equation (11) leads to the expression

$$\frac{I(\mathrm{O_K})}{I(\mathrm{V_{L_{23}}})} = \frac{\sigma_{\mathrm{O\,1s}}}{\sigma_{\mathrm{V\,2p}}} \frac{(n_g - n_d)}{(10 - n_g)} \tag{12}$$

which is independent of the stoichiometry (a and b). If we further assume the photoabsorption cross-sections to be purely atomic properties, independent of the actual compound, they will drop out of a comparison between the various vanadium oxides. We thus find the normalized O K absorption weight to depend directly on n_g, and, in particular, to scale with the deviation of n_g from the purely ionic 3d occupation n_d. Taking n_g from our cluster-model results in table 3 yields theoretical relative O K-to-V L_{23} intensity ratios of 1.8:1.4:1 for $\mathrm{V_2O_5}$:$\mathrm{VO_2}$:$\mathrm{V_2O_3}$, in rather good agreement with the experimental values 2.2:1.3:1 extracted from the XAS spectra in figure 7. We take this good agreement as an independent confirmation of our cluster-model results.

3.2.2. ResPES of the valence band near the V L_{23} threshold. Figure 9 presents valence band spectra of $\mathrm{V_2O_3}$ (figure 9(a)) and $\mathrm{V_2O_5}$ (figure 9(b)) measured at photon energies near the V 2p threshold (marked by the arrows in figure 7). All of the spectra are corrected for a Shirley-type background, and are normalized to the intensity of the O 2s structure at $E_B \approx 22$ eV; at some photon energies, this was difficult to achieve due to interference with an LVV Auger signal.

In both oxides the intensity of the O 2p band centred at around 5–6 eV binding energy shows a pronounced enhancement which, in agreement with our cluster-model results, reflects a strong V 3d admixture with this spectral region, if interpreted as a pure ResPES effect. Unfortunately, however, the spectra contain additional contributions from incoherent LVV Auger processes, which can make the interpretation of ResPES data rather ambiguous, as was argued from a detailed analysis of 'giant resonances' in some late TMs and their oxides [56, 57]. These incoherent Auger decays lead to a different (two-hole) final state

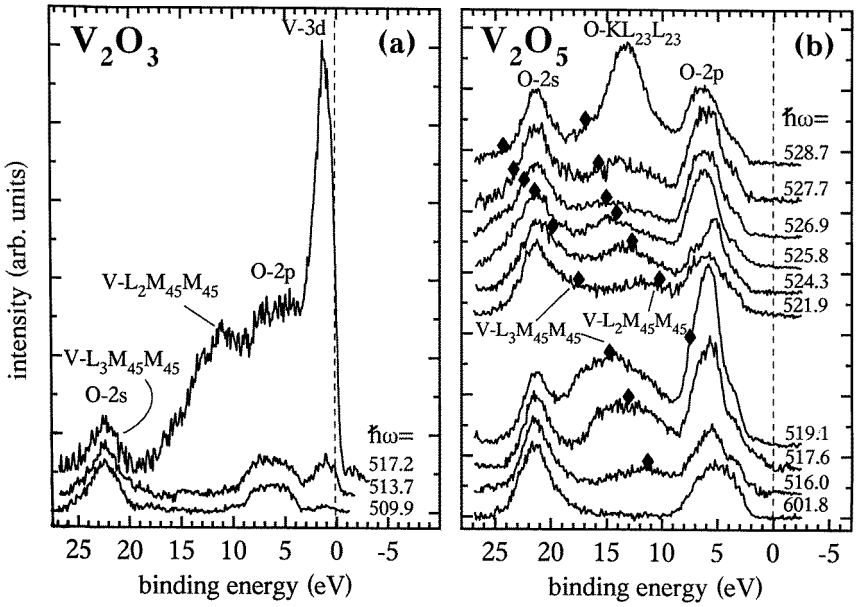

Figure 9. (a) Resonant photoemission at the V 2p threshold for V_2O_3. The upper and lower spectra correspond to on- and off-resonance systems, respectively. (b) Resonant photoemission at the V 2p threshold for V_2O_5. The lower spectrum corresponds to an off-resonance system. The diamonds indicate the positions of the incoherent V LVV Auger emissions. The photon energies are given in eV on the right-hand side of the spectra.

d^{n-2} which, in principle, should be distinguishable from the coherent ones (d^{n-1}) on the basis of its photon energy dependence, because they appear at constant kinetic energy and thus shift with photon energy, whereas the true resonance appears at constant binding energy. However, if the two processes cover a relatively broad spectral range (e.g. because of multiplet effects), an unambiguous decomposition of the spectra is hardly possible. In the case of the vanadium oxides, this prevents us from carrying out a more quantitative analysis of the spectra. Nonetheless, the data in figure 9 clearly show that the observed intensity increase is not exclusively caused by incoherent Auger weight (whose centre position is marked by the diamonds in figure 9(b)), but that there is also intrinsic resonant photoemission enhancement. Moreover, the occurrence of incoherent Auger processes of the 2p3d3d type already indicates that the 3d occupation in V_2O_5 must be different from 0, again supporting our conclusion that there is a strong V 3d–O 2p overlap.

For V_2O_5, the intensity of the 'O 2p'-related valence band part follows qualitatively the photon energy dependence of the absorption, with maxima at $\hbar\omega \approx 519.1$ eV and $\hbar\omega \approx 525.8$ eV. The resonance is strongest on the high-binding-energy side of the 'O 2p' band, indicating a strong V 3d admixture, and is much less pronounced towards lower binding energy. These findings are in good agreement with recent band-structure calculations [58, 59] which find the 'O 2p' band to consist of strongly hybridized V 3d–O 2p bonding states at higher binding energies and of non-bonding O 2p character (with some admixture of V 4sp states) at lower energies. Similar results have been observed in 3p–3d ResPES experiments by Shin *et al* [49] who explained the resonant behaviour of the 'O 2p' band as manifesting a strong contribution of the $d^1\underline{L}$ configuration in the ground state, in accordance with the results of our cluster-model calculations (cf. figure 6).

For V_2O_3, we observe, additionally to the resonance in the 'O 2p' band, a strong enhancement of the feature at $E_B \approx 1$ eV. This agrees again well with ResPES experiments on the V 3p threshold [48] and band-structure calculations, which identify the 1 eV peak as of V 3d character with a strong O 2p admixture, and obtain a considerable V 3d contribution to the 'O 2p' band [58].

4. Conclusions

The electronic structure of the vanadium oxides V_2O_5, VO_2, and V_2O_3 is determined predominantly by the strong hybridization between V 3d and O 2p orbitals. The interpretation of vanadium core-level spectra in the framework of a simple cluster model based on the AIH leads to the result that the effective hybridization energy $V_{eff} = \sqrt{n_h}V$ is significantly larger than the charge-transfer energy Δ and the d–d correlation energy U_{dd} of the model, although the latter two remain of importance. A large contribution from several basis configurations $|d^{n+q}\underline{L}^q\rangle$ to the initial state and from $|\underline{c}d^{n+q}\underline{L}^q\rangle$ to the photoemission final states yields V 3d occupation numbers much higher than the numbers expected in a purely ionic picture based on formal valencies. This also means that neither the ground state nor the final states can be characterized by a single dominant configuration, as is possible for the late TM compounds, for which covalency plays a minor role. The strong influence of hybridization in early 3d TMOs is supported by XAS and ResPES data, where the occurrence of O K absorption intensity itself and the resonating behaviour of the 'O 2p' band at the V L_{23} threshold confirm a strong mixing of V 3d and O 2p states.

The absence of a V 3s exchange splitting in the d^0 compound V_2O_5 indicates that the total 3d spin $S = 0$ expected in the ionic limit remains unchanged by the hybridization, although it does lead to a non-zero d occupation. Finite exchange splittings are observed in the other two oxides, even though the magnetic susceptibility of VO_2 shows no behaviour characteristic of the existence of local moments. This demonstrates that, for these compounds, the relationship of the 3s exchange splitting to the d occupation, the valence spin, and the macroscopic magnetic behaviour is little understood, and requires further theoretical elucidation.

These results, which reveal the importance of hybridization and covalency in the vanadium oxides, demand a reconsideration of the standard classification of early TMOs as simple Mott–Hubbard compounds (with U_{dd} as the single most important parameter), which we believe, in agreement with previous studies [19, 20, 21, 48], to be no longer justified. Instead, their electronic structure appears to be determined by a delicate balance between covalency, d–d correlation, and charge-transfer energy, which may also be ultimately responsible for the rich phase diagrams encountered for these compounds.

Acknowledgments

The authors would like to express their gratitude to Professor S Horn (Universität Augsburg) for providing the V_2O_5 single crystals, A Frantzen (Universität des Saarlandes) for the preparation of the VO_2 and V_2O_3 samples, and C Ogglesby (Bell Laboratories) for providing additional V_2O_3 crystals. We also acknowledge the assistance by the BESSY staff, especially Ch Hellwig and Ch Jung. We further wish to thank P Blaha and P Dufek (TU Wien), and A Kotani, T Uozumi, and H Ogasawara (University of Tokyo) for many valuable discussions. This work was supported by the Bundesministerium für Bildung und Forschung (BMBF) and by the Deutsche Forschungsgemeinschaft (DFG).

References

[1] Shin S, Suga S, Taniguchi M, Fujisawa M, Kanzaki H, Fujimori A, Daimon H, Ueda Y, Kosuge K and Kachi S 1990 *Phys. Rev.* B **41** 4993
[2] Allen P B, Wentzcovitch R M, Schulz W W and Canfield P C 1993 *Phys. Rev.* B **48** 4359
[3] *Gmelin Handbuch der Anorganischen Chemie* (Berlin: Springer)
[4] Hüfner S 1985 *Z. Phys.* B **61** 135
[5] Carter S A, Rosenbaum T F, Metcalf P, Honig J M and Spalek J 1993 *Phys. Rev.* B **48** 16 841
[6] Mott N F 1949 *Proc. Phys. Soc.* A **62** 416
Mott N F 1956 *Can. J. Phys.* **34** 1356
Mott N F 1961 *Phil. Mag.* **6** 287
[7] Hubbard J 1963 *Proc. R. Soc.* A **276** 238
Hubbard J 1964 *Proc. R. Soc.* A **277** 237
Hubbard J 1964 *Proc. R. Soc.* A **281** 401
[8] Thomas G A, Rapkine D H, Carter S A, Millis A J, Rosenbaum T F, Metcalf P and Honig J M 1994 *Phys. Rev. Lett.* **73** 1529
[9] Rice T M, Launois H and Pouget J P 1994 *Phys. Rev. Lett.* **73** 3042
[10] Wentzcovitch R M, Schulz W W and Allen P B 1994 *Phys. Rev. Lett.* **72** 3389
[11] Sawatzky G A and Allen J W 1984 *Phys. Rev. Lett.* **53** 2339
[12] Lee G and Oh S-J 1991 *Phys. Rev.* B **43** 14 674
[13] Okada K and Kotani A 1989 *J. Phys. Soc. Japan* **58** 2578
[14] Zaanen J, Sawatzky G A and Allen J W 1985 *Phys. Rev. Lett.* **55** 418
[15] van der Laan G, Westra C, Haas C and Sawatzky G A 1981 *Phys. Rev.* B **23** 4369
[16] Zaanen J, Westra C and Sawatzky G A 1986 *Phys. Rev.* B **33** 8060
[17] Ghijsen J, Tjeng L H, van Elp J, Eskes H, Westerink J, Sawatzky G A and Czyzyk M T 1988 *Phys. Rev.* B **38** 11 322
[18] Parlebas J C 1992 *J. Physique* **2** 1369
[19] Uozumi T, Okada K and Kotani A 1993 *J. Phys. Soc. Japan* **62** 2595
[20] Park J-H 1994 *PhD Thesis* Michigan State University, East Lansing, MI
[21] Allen J W *et al* 1995 *The Hubbard Model* ed D Baeriswyl *et al* (New York: Plenum) p 357
[22] Anderson P W 1961 *Phys. Rev.* **124** 41
[23] Bocquet A E, Mizokawa T, Morikawa K, Fujimori A, Barman S R, Maiti K, Sarma D D, Tokura Y and Onoda M 1996 *Phys. Rev.* B **53** 1161
[24] Uozumi T, Okada K, Kotani A, Zimmermann R, Steiner P, Hüfner S, Tezuka Y and Shin S 1997 *J. Electron Spectrosc. Relat. Phenom.* **83** 9
[25] Berliner Elektronenspeicherring-Gesellschaft für Synchrotronstrahlung mbH 1993 *Research at BESSY—a User's Handbook*
[26] Shirley D A 1972 *Phys. Rev.* B **5** 4709
[27] Zimmermann R 1996 *PhD Thesis* Universität des Saarlandes, Saarbrücken
[28] The Gaussians and Lorentzians used to fit the spectra only serve to determine the integrated weights and peak positions. They are not meant to reproduce realistic line profiles, which e.g. for metallic V_2O_3 may contain an asymmetry due to electron–hole-pair shake-up (the Doniach–Sunjic line-shape) or a low-energy plasmon satellite due to the narrow conduction band. The neglect of these effects is of marginal importance for the cluster model parameters derived here, with a possible error certainly smaller than the uncertainty in the inelastic background subtraction.
[29] Manne R and Åberg T 1970 *Chem. Phys. Lett.* **7** 282
[30] Imer J-M and Wuilloud E 1987 *Z. Phys.* B **66** 153
[31] Slater J C 1960 *Quantum Theory of Atomic Structure* (New York: McGraw-Hill)
[32] Okada K, Kotani A, Kinsinger V, Zimmermann R and Hüfner S 1994 *J. Phys. Soc. Japan* **63** 2410
[33] Tanaka A and Jo T 1994 *J. Phys. Soc. Japan* **63** 2788
[34] Okada K and Kotani A 1992 *J. Phys. Soc. Japan* **61** 449
[35] Hüfner S 1994 *Adv. Phys.* **43** 183
[36] Matthew J A D and Komninos Y 1975 *Surf. Sci.* **53** 716
[37] Reinert F, Kumar S, Steiner P, Claessen R and Hüfner S 1994 *Z. Phys.* B **94** 431
[38] Sawatzky G A and Post D 1979 *Phys. Rev.* B **20** 1546
[39] McFeely F R, Kowalczyk S P, Ley L and Shirley D A 1972 *Phys. Lett.* **49A** 301
[40] Kinsinger V, Zimmermann R, Hüfner S and Steiner P 1992 *Z. Phys.* B **89** 21
Kinsinger V, Sander I, Steiner P, Zimmermann R and Hüfner S 1990 *Solid State Commun.* **73** 527

[41] van Vleck J W 1934 *Phys. Rev.* **45** 405
[42] Shirley D A 1975 *Phys. Scr.* **11** 117
[43] Menth A and Remeika J P 1970 *Phys. Rev.* B **2** 3756
[44] Shin S, Tezuka Y, Kinoshita T, Kakizaki A, Ishii T, Ueda Y, Jang W, Takei H, Chiba Y and Ishigame M 1992 *Phys. Rev.* B **46** 9224
[45] Pouget J P, Lederer P, Schreiber D S, Launois H, Wohlleben D, Casalot A and Villeneuve G V 1972 *J. Phys. Chem. Solids* **33** 1961
[46] van Acker J F, Stadnik Z M, Fuggle J C, Hoekstra H J W M, Buschow K H J and Stroink G 1988 *Phys. Rev.* B **37** 6827
[47] Davis L C 1982 *Phys. Rev.* B **25** 2912
[48] Smith K E and Henrich V E 1988 *Solid State Commun.* **68** 29
Smith K E and Henrich V E 1988 *Phys. Rev.* B **38** 9571
[49] Shin S, Tezuka Y, Ishii T and Ueda Y 1993 *Solid State Commun.* **87** 1051
[50] de Groot F M F, Fuggle J C, Thole B T and Sawatzky G A 1990 *Phys. Rev.* B **42** 5459
de Groot F M F, Fuggle J C, Thole B T and Sawatzky G A 1990 *Phys. Rev.* B **41** 928
de Groot F M F, Grioni M, Fuggle J C, Ghijsen J, Sawatzky G A and Petersen H 1989 *Phys. Rev.* B **40** 5715
de Groot F M F 1991 *PhD Thesis* University of Nijmegen
[51] Soriano L, Abbate M, Fuggle J C, Jimeénez M A, Sanz J M, Mythen C and Padmore H A 1993 *Solid State Commun.* **87** 699
[52] Goering E, Müller O, denBoer M L and Horn S 1994 *Physica* B **194–196** 1217
Goering E, Müller O, Klemm M, Urbach J P, Petersen H, Jung C, denBoer M L and Horn S 1995 *Physica* B **208+209** 300
Goering E, Müller O, Klemm M, denBoer K L and Horn S 1997 *Phil. Mag.* B **75** 229
[53] Uozumi T 1995 *PhD Thesis* University of Tokyo
[54] Yamaguchi T, Shibuya S, Suga S and Shin S 1982 *J. Phys. C: Solid State Phys.* **15** 2641
[55] van der Laan G and Kirkman I W 1992 *J. Phys.: Condens. Matter* **4** 4189
[56] López M F, Höhr A, Laubschat C, Domke M and Kaindl G 1992 *Europhys. Lett.* **20** 357
López M F, Laubschat C and Kaindl G 1993 *Europhys. Lett.* **23** 538
López M F, Laubschat C, Gutiérrez A, Höhr A, Domke M, Kaindl G and Abbate M 1994 *Z. Phys.* B **95** 9
[57] Tjeng L H, Chen C T, Ghijsen J, Rudolf P and Sette F 1992 *Phys. Rev. Lett.* **67** 501
[58] Blaha P and Dufek P 1995/96 private communication (TU Wien, Austria)
[59] Eyert V and Höck K-H 1998 *Phys. Rev.* B **57** 12 727